Case Studies in Thermal Engineering 72 (2025) 106330

Contents lists available at ScienceDirect

Case Studies in Thermal Engineering

journal homepage: www.elsevier.com/locate/csite

In situ performances of direct absorption solar collector based on Ag NPs-rGO hybrid nanofluid

Angel Huminic [*], Gabriela Huminic [**]

Transilvania University of Brasov, Mechanical Engineering Department, 29, Bulevardul Eroilor, 500036, Brasov, Romania

ARTICLE INFO

Handling Editor: Dr Y Su

Keywords:
DASC
CFD
Water-ethylene glycol
Ag NPs –rGO sheets
In situ experiments

ABSTRACT

Recent research on direct absorption solar collectors (DASCs) follows a general upward trend due to continuous development of new materials and working fluids, which provide opportunities for improvement of their performances regarding conversion of solar energy into thermal energy. Using of nanofluids as absorbent and heat-conducting media has proven to be an efficient method to increase the effectiveness of these collectors, mainly due to higher optical properties, particularly absorption, compared to typical working fluids, e.g. water, ethylene-glycol or oil, which absorb weakly the sunlight. In this study, a DASC prototype has been designed and optimized using CFD, and later fabricated and tested using Ag NPs + rGO hybrid nanofluid in water-ethylene glycol solution. To evaluate the effect of the nanoparticles, experiments were simultaneously carried out for two DASCs, the second one being filled with simple water-ethylene glycol solution, and used also as reference DASC. In order to achieve relevant data, the investigations were performed under outdoor conditions during summer season, for several representative flow rates of the working fluid. The results show that the efficiency of DASC using hybrid nanofluid increases significantly, the maximum relative enhancement being 74.1 %. In addition, instantaneous and accumulative energies delivered are about 44 % and 98 % respectively higher than for DASC using water-ethylene glycol solution. Based on data collected, a correlation for Nusselt number is proposed.

Nomenclature

A	absorber area, m^2	σ	Stefan-Boltzmann constant, W/m^2K^4
c_p	specific heat, J/kgK	θ	tilt angle
D_h	hydraulic diameter, m	ζ	head loss coefficient
G_t	solar irradiance, W/m^2		
h	heat transfer coefficient, W/m^2K	*Subscript*	
H	height of collectors, m	a	ambient
k	thermal conductivity, W/mK	air	air
L	length of collector, m	c	convection
$\dot{m}$	mass flow rate, kg/s	d	dynamic
n	number of ribs	g	glass
p	pressure, Pa	h	collector thickness

(*continued on next page*)

* Corresponding author.
** Corresponding author.
E-mail addresses: angel.h@unitbv.ro (A. Huminic), gabi.p@unitbv.ro (G. Huminic).

https://doi.org/10.1016/j.csite.2025.106330
Received 10 February 2025; Received in revised form 24 April 2025; Accepted 13 May 2025
Available online 13 May 2025

(*continued*)

Q_{loss}	heat losses, W	*hnf*	hybrid nanofluid
$\dot{Q}_u$	useful power output, W	*i*	inside
T	temperature, K	*in*	inlet
v	velocity, m/s	*out*	outlet
$\dot{V}$	flow rate, l/min	*r*	radiation
Pr	Prandtl number	*t*	total
Re	Reynolds number	*w*	water
		wh	water heater
Greek symbols:			
δ	width of the ribs, m	*Abbreviations:*	
Δ	space between ribs, m	*Ag NPs*	silver nanoparticles
ε_g	glass emissivity	*CFD*	Computational Fluid Dynamics
ϕ	volume fraction	*DASCs*	Direct Absorption Solar Collectors
μ	dynamic viscosity, kg/m s	*FPSCs*	Flat-Plate Solar Collectors
ρ	density, kg/m^3	*rGO*	reduced graphene oxide
		W + EG	water and ethylene glycol

1. Introduction

Currently, the solar energy is one of the most exploited renewable energy source because it is inexhaustible and nonpolluting compared to coal, petroleum and natural gas. Although apparently it represents a free source of energy, its harvesting, conversion and storage still involve high costs. The most common devices that use the solar energy for heating applications (solar water heaters and/or house heating) are flat-plate solar collectors (FPSCs). These collectors require quite large areas to satisfy the domestic needs, which lead to significant heat losses by convection and radiation heat transfer. A reliable alternative to the flat-plate solar collectors proved to be direct absorption solar collectors (DASCs) due to new advanced heat transfer fluids in which the surface area and the heat losses are significantly diminished. The advanced heat transfer fluids, also called nanofluids, consist on common liquids, such water, ethylene-glycol or oil that generally have poor absorption characteristics, into which nano-sized solid particles are embedded. Employing nanofluids instead of ordinary fluids, the efficiency of the DASCs is improved significantly, because these fluids exhibits enhanced thermal and optical properties, namely thermal conductivity [1–3] and transmittance, absorbance and extinction coefficients [4,5].

So far, there are studies devoted to the efficiency of DASCs, using both experimental and numerical methods. In addition, few nanofluids, such as silver, carbon nanotubes, magnetite and graphite were examined. Thus, Otanicar et al. [6] studied numerically and experimentally the influence of various water-based nanofluids (graphite, Ag and CNT) on efficiency of DASCs. Their results indicate an improvement of efficiency up to 55.5 %, 57.5 % and 54.0 % for graphite, Ag and CNT respectively. In a subsequent numerical study, Otanicar et al. [7] reported a maximum improvement in DASCs efficiency of 71 % and 41.5 % for graphite/water and Ag/water nanofluids. Concentrations of these nanofluids were 0.4–1.0 vol % for graphite and 0.1 vol % Ag NPs. The effect of 0.125 vol% of graphite dispersed into therminol VP-1 on the performances of DASCs was numerical studied also by Taylor et al. [8], reporting an enhancement up to 11 % in efficiency compared to the base fluid. Ladjevardi et al. [9] developed a numerical code to investigate the performances of DASCs using water and graphite nanofluids with volume concentrations from 0.000025 % to 0.0025 %. They found that the DASCs using 0.000025 vol% graphite could absorb more than 50 % of incident irradiation energy compared to water, that could absorb only 27 %. Luo et al. [10] investigated both numerically and experimentally the performances of the DASCs using C, TiO_2, Al_2O_3, Ag, Cu, SiO_2, graphite, and CNT dispersed into Texatherm oil. Their results show that the efficiency for all studied nanofluids were in the following order of nanoparticles: C $\approx$ Ag $\approx$ Al_2O_3 > SiO_2 $\approx$ 0.01 % Cu > 0.025 %Cu > TiO_2. In addition, they reported an improvement in photo-thermal efficiency of 122.7 % for 0.01 vol % graphite nanofluid, and 117.5 % when 0.5 vol % Al_2O_3 nanofluid was used.

Gorji and Ranjbar [11] performed a CFD study in order to find the optimum geometry of a simple box DASC using graphite/water nanofluid with concentrations from 0.05 to 1.0 vol % and reported a maximum efficiency of 78.06 % for the optimal geometry (L = 12.08 cm, W = 5 cm, H = 2 cm and 0.1 vol %). In another study, Gorji and Ranjbar [12] carried out both numerical and experimental studies regarding the graphite, magnetite and silver nanofluids used in DASCs and reported that the thermal efficiencies is improved by using nanofluids in a range of 33 %–57 % compared to the base fluid (water). Gorji and Ranjbar [13] also numerically studied the influence of graphite, magnetite and silver nanoparticle concentrations, flow rate and incident radiative flux on the DASCs thermal performance. Their results pointed out an improvement in thermal efficiency of 84.6 %, 94.3 % and 51.4 % for DASCs using graphite, magnetite and silver NPs.

Liu et al. [14] performed a theoretical and experimental study in laboratory conditions on graphene/[H_{mim}]BF_4 (ionic liquid) nanofluid with various concentrations (from 0.0005 wt% to 0.01 wt%) used in DASCs. They found that efficiency increases with the intensity of solar radiation and the distance to receiver, but it diminishes with concentration of graphene. They also reported that a lower amount of graphene dispersed into ionic liquid (0.0005 wt%) can enhance the DASC efficiency. Vakili et al. [15] experimentaly investigated in outdoor conditions the performances of DASCs using graphene nanoplatelets nanofluid According to their results, the efficiency of tested DASCs increases up to 83.5 %, 89.7 % and 93.2 % when nanofluid is employed with mass concentrations of 0.0005 %, 0.001 % and 0.005 % respectively. Bandarra Filho et al. [16] carried out a study regarding the effectiveness of the DASCs using silver nanofluid and found that performance increases up to 144 % using 6.5 ppm silver NPs.

An experimental and numerical study was carried out by Delfani et al. [17] to enhance the performance of DASCs wits MWCNT-water and ethylene glycol mixture. They investigated the effects of the volume fraction of MWCNT, flow rate and internal

surfaces (black and reflective) on DASC efficiency. Their results indicate that the efficiency is improved up to 29 % if the volume fraction and the flow rate are increased. In another study, Karami et al. [18] investigated experimentaly the effect of polyvinylpyrroledone (PVP)-coated silver nanofluid on DASCs. The experiments were performed for various Ag volume fractions (250, 500, and 1000 ppm), mass flow rates (0.0075, 0.015, 0.0225 kg/s) and tilt angles (20, 35, 50°) of DASC, and the results show that the efficiency increases with flow rate and decreases with tilt angle when Ag nanofluid is used. Based on collected data, two correlations for thermal efficiency were developed. Struchalin et al. [19] performed a numerical and experimental study on performance of a tubular DASC using MWCNTs dispersed in a water-ethanol mixture. They investigated the effect of volume concentration (0.0015-0.082 wt %), flow rate (2–10 l/min), temperature differences and radiant heat fluxes on DASC efficiency, and found out that the thermal efficiency was within the range 80–97 % for 0.01 wt%., which was the optimum concentration. Kumar et al. [20] experimentally studied the performance of DASC using Au plasmonic nanofluid under outdoor conditions. Their results indicated a maximum thermal performance improvement of 31 % compared to the base fluid at a mass flow rate of 0.017 kg/s.

Recently, hybrid nanofluids, which consist of two or more sorts of nanoparticles or composite nanopowders dispersed into a base fluid, were considered in non-concentrating solar collectors using flat plates [21,22], heat pipe evacuated tubes [23], direct absorption [24,25] and concentrating solar collectors (linear Fresnel reflectors) [26]. Studies performed on these devices using hybrid nanofluids reveal the increasing of their performances due to improved optical properties of hybrids compared to nanofluids. Regarding the potential of the hybrid nanofluids in direct absorption solar collectors there are numerous studies that have investigated both the optical properties and photo-thermal conversion characteristics [27–31] in laboratory conditions, but only Karami et al. [24] investigated experimentally the potential of full-scale DASCs in outdoor conditions. They studied the performances of a direct absorption solar collector using Fe_3O_4/SiO_2 nanofluid with respect to both effect of volume fraction (500, 1000 and 2000 ppm) and mass flow rate (0.0075, 0.015, 0.0225 kg/s) on thermal and exergetic efficiency. They reported an enhancement of 21.7 % and 66.4 % in thermal and exergetic efficiency for 2000 ppm Fe_3O_4/SiO_2 nanofluid and mass flow rate of 0.0225 kg/s. Hachicha and Said [25] carried out a numerical study on capabilities of DASC using Cu–Al_2O_3 hybrid nanofluid. The volume concentrations of Cu were 0.01 %, 0.04 %, 0.07 %, and 0.1 %, while the volume concentrations of Al_2O_3 were 0.05 %, 0.1 %, 0.5 %, and 1 %. Their results indicated that for lower volume concentrations of Cu particles, the addition of Al_2O_3 particles contributes to improvement of DASC efficiency, while at larger volume concentrations of Cu particles, Al_2O_3 particles have a minor importance.

Since most existing research has been limited to small-scale laboratory experiments that may not accurately reflect the performance of DASCs under real-world conditions, and given the lack of experimental studies on full-scale DASCs utilizing hybrid nanofluids, as well as the limited attention paid to optimizing their internal geometry, particularly under realistic operating conditions, this study proposes a two-step approach to address these limitations. First, a comprehensive numerical investigation using computational fluid dynamics (CFD) is conducted to optimize the internal geometry of the DASC by introducing ribbed flow channels. Several rib configurations are analyzed under laminar flow conditions, and the optimal number of ribs is identified to enhance thermal performance. Based on these simulation results, a large-scale DASC prototype incorporating the optimal rib design and utilizing Ag NPs + rGO/water-ethylene glycol hybrid nanofluid as working fluid is manufactured and tested under realistic outdoor conditions. This integrated approach provides both practical insights and design guidelines for the development of high-efficiency DASCs.

Silver nanoparticles (Ag NPs) and reduced graphene oxide (rGO) nanosheets were chosen for developing a novel hybrid nanofluid, due to their exceptional thermo-physical and optical characteristics that make them highly suitable for solar collector applications. Ag NPs exhibit a strong localized surface plasmon resonance (LSPR), which significantly enhances the absorption of incident solar radiation, while also offering high thermal conductivity (~429 W/m·K). On the other hand, rGO nanosheets, with their inherently black color and broad-spectrum optical absorption, exhibit ultra-high thermal conductivity (~3000 W/m·K). The combination of Ag NPs and rGO nanosheets creates a synergistic effect, where the LSPR-induced light absorption of Ag NPs is amplified by the optical and thermal properties of rGO. This hybrid system thus presents a highly promising approach to improving the efficiency of direct absorption solar collectors (DASCs), making both materials exceptionally well-suited for this application. To evaluate the effect of the hybrid

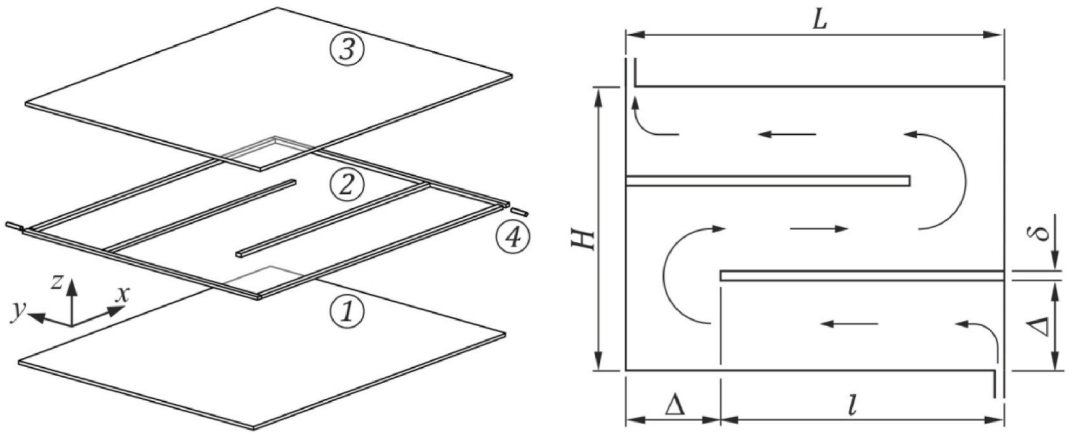

Fig. 1. Design of DASC

nanofluids, experiments were simultaneously carried out for two DASCs, one of them being filled with simple water-ethylene glycol solution, used as reference. In order to achieve relevant data, the investigations were performed in outdoor conditions during summer season in Brasov city, Romania, for several representative flow rates of the working fluid.

2. Design and optimization of DASC

For the solar panel, the simplest geometry was considered, namely a flat box made from transparent glass sheet of 6 mm thickness with the following properties: density $\rho_g = 2430\ kg/m^3$, specific heat $c_{p_g} = 828\ J/kg\ m$ and thermal conductivity $k_g = 1.06\ W/\ m\ K$. As shown in Fig. 1 for DASC with two ribs, it consist of the upper plate 1, side frames and ribs 2, the lower plate 3 and the inlet and outlet pipes 4, all glued together, then insulated in the sides and bottom. The ribs were considered in order to achieve flows as through a serpentine channel.

The main dimensions are $L = 650\ mm$ (width), $H = 500\ mm$ (high) and $\delta = 10\ mm$ (width of the ribs). For these dimensions, a maximum amount of 5 L of working fluid is required for the all equipments necessary for experiments. Space between ribs Δ and their length l and were computed with Eqs. (1) and (2):

$$\Delta = \frac{H - n\,\delta}{n+1} \tag{1}$$

$$l = L - \Delta \tag{2}$$

Horizontal layout of DASC (a larger base) has been considered in order to minimize the number of ribs, also to attain longer channels between them, and consequently more uniform flows as possible. In addition, the inlet is on the lower side, perpendicular to the channels, in order to fill the entire volume of DACS with liquid during its operation.

In the next step of the design process, optimum number of the ribs has been examined. Thus, using the capabilities of ANSYS FLUENT, a state-of-the-art CFD software, a numerical study was performed for DASCs with $n = 0, 2, 4\ 6, 8$ and 10 ribs, working with water in laminar regime for three values of the flow rate: $\dot{V}_1 = 0.4\ l/min$, $\dot{V}_2 = 0.75\ l/min$ and $\dot{V}_3 = 1.1\ l/min$. The minimum value of the flow rate was computed according to the European Standard EN 12975-2 regarding the outdoor test of solar collectors, which stipulate a mass flow rate of the heat transfer fluid of $0.02\ kg/s\ m^2$ per square meter of collector area. For the CFD simulations, water at $293.15\ K$ ($20\ ^\circ C$) was considered as working fluid with $\rho_w = 998.2\ kg/m^3$ (density), $c_{p_w} = 4182\ J/kg\ K$ (specific heat), $k_w = 0.6\ W/\ m\ K$ (thermal conductivity) and $\mu_w = 0.001003\ kg/m\ s$ (dynamic viscosity). Reynolds number for each flow regime was computed with the Equation

$$Re = \frac{\rho_w\, v_{in}\, d_{in}}{\mu_w} = \frac{\rho_w}{\mu_w}\,\frac{4\dot{V}}{\pi\, d_{in}}, \tag{3}$$

and the values are $Re_1 = 1410$, $Re_2 = 2640$ and $Re_3 = 3880$. Hexahedral grids were generated for all computational domains. The sides of the elements along x and y axis are constant, of 1 mm, and the height of elements along z-axis are variable, smaller towards the DASCs faces, as shown in Fig. 2. This approach allows fast and fully orthogonal generation of elements. Several tests regarding results using 5, 7, 9 and 11 elements in depth were performed, and based on the results, 9 elements were considered along z-axis.

Navier-Stokes and energy equations together with solar load of constant irradiation $G_t = 1000\ W/m^2$ were employed to simulate flow and heat transfer inside the DASC.

The following boundary conditions were considered for the frontiers of the computational domains.

- velocity v_{in}, according to the flow rate, normal to the inlet boundary, at $T_{in} = 293.15\ K$ ($t_{in} = 20\ ^\circ C$),
- zero gauge pressure on outlet, $p_{out} = 0\ Pa$, having as reference the atmospheric pressure $p_{air} = 101325\ Pa$,
- convection ($h = 10\ W/m^2K$, air to DASC heat transfer coefficient, and $T_{air} = 303.15\ K$ ($t_{air} = 30\ ^\circ C$), outdoor temperature) for the upper surface, which also is the subject of the solar radiation,
- adiabatic walls for the rest of the boundaries.

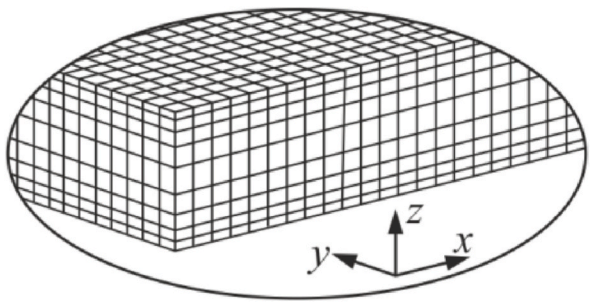

Fig. 2. Detail of the used mesh.

The mass flow rate $\dot{m}_{out}$ and temperature T_{out} at the outlet have been monitored during the solutions, and the analyses were considered complete when these parameters stabilized during the final iterations and the residuals of the variables reached at least the limit 1e-004. To evaluate the results, efficiency (η) of DASCs and head loss coefficient (ζ) were computed with the Eqs:

$$\eta = \frac{\dot{Q}_u}{A_A G_t} = \frac{\dot{m}\, c_{p_w}(T_{out} - T_{in})}{A_A\, G_t}, \tag{4}$$

$$\zeta = \frac{\Delta p_t}{p_{din}} = \frac{p_{tout} - p_{tin}}{\frac{\rho_w\, v_{in}^2}{2}} \tag{5}$$

where the area of DASCs under the influence of the solar irradiation is

$$A_A = H\, L - n\, \delta\, l. \tag{6}$$

Fig. 3 depicts these results. As shown, ribs are not necessary for low flow rates, when DASCs' efficiency decreases slightly from 0.38 (if there are no ribs) to near 0.37 for 10 ribs. Ribs proved to be necessary for larger flow rates when, as assumed, they contribute to the uniformity of the flow through collectors, as depicted in Figs. 4 and 5. For larger flow rates, DASCs' efficiency increases with the number of used ribs. For all analyses, variation of the efficiency become insignificant if $n \geq 6$. In addition, head loss coefficient variation increases significantly, more than 20 % if $n > 6$.

Fig. 4 shows comparatively the variation of temperature (same interval, 50 contours) on the upper face of DASCs with no ribs and 6 ribs and the aspect of 3D streamlines inside them for the third value of flow rate.

In order to understand better how heat is transmitted inside the DASC with 6 ribs, Fig. 5 depicts same variation of temperature but within the interval specific to this case, together with the velocity profile of the working fluid in the collector's symmetry plane *yoz*.

As shown, inside of the DASC with no ribs the temperature increases very much around lower left corner due to a large recirculation vortex what develops in this area. Unlike this phenomenon, the flow becomes quickly uniform when six ribs are used, as revealed by the aspect of the streamlines and the velocity profile inside the channels of DACS. As depicted, several significantly smaller vortices develop only in the first channel. In addition, no hot area is visible for this situation.

Thus, for the cases studied, the optimal number of ribs was found to be n = 6, and this configuration was selected for the DASC manufacturing. For this layout, an experimental test was conducted using pure water at a volumetric flow rate of $\dot{V}_3 = 1.1\ l/\ min$, as described in the following section. The experimental thermal efficiency was $\eta = 0.389$ (38.9 %), while the CFD simulation predicted an efficiency of $\eta = 0.378$ (37.8 %). The resulting difference of 2.8 % between the experimental and numerical results demonstrates the accuracy and reliability of the CFD methodology employed in this study.

3. Experimental facilities used to test of DASC

3.1. Experimental facilities and test procedure of DASC

After the design and optimization stages, several prototypes of DASCs were manufactured, and later tested. In order to minimize heat losses from back and sides of the solar collectors, these were isolated with neoprene block of 8 mm thickness and a heat reflective thermal panel of 4 mm made of polyester with aluminum foil, specifically designed to reflect radiant heat and minimize heat transfer. Two collectors were placed on a frame at 45° angle of inclination in order to test simultaneously their performances, also to achieve conclusive results regarding variations of monitored parameters in similar conditions.

Fig. 6 depicts schematic diagram of experimental layout used for experiments. As shown, it consists of two solar collectors in connection with two solar stations Hewalex ZPS 18e-01 ECO, specifically designed for operating of solar installations. They contain all necessary components and accessories, such pump with electronic speed control (*P*), flow meter (*FM*), pressure gauge manometer (*M*),

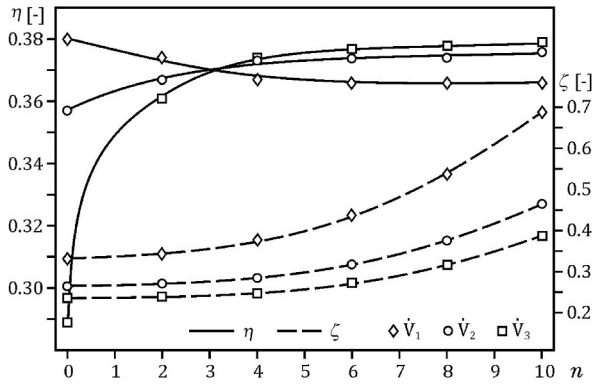

Fig. 3. DASC efficiency and head loss coefficient with the number of ribs.

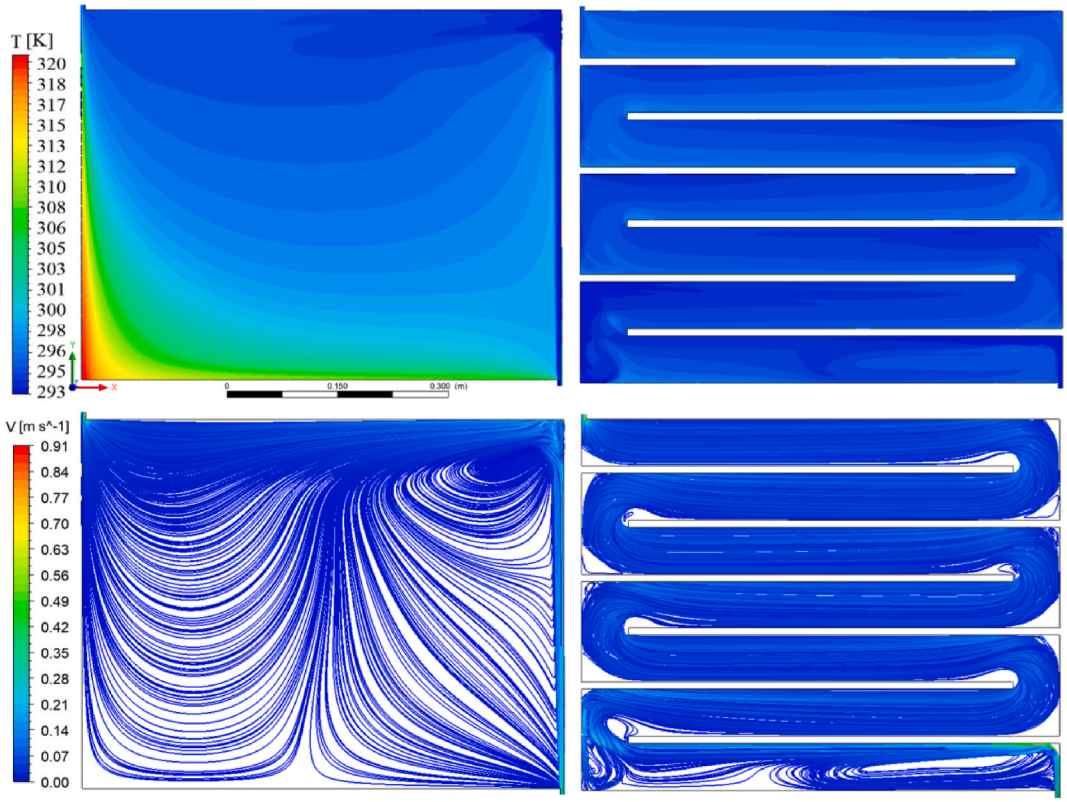

Fig. 4. *Temperature variation and aspect of 3D streamlines for* DASCs with 0 and 6 ribs, $\dot{V}_3$

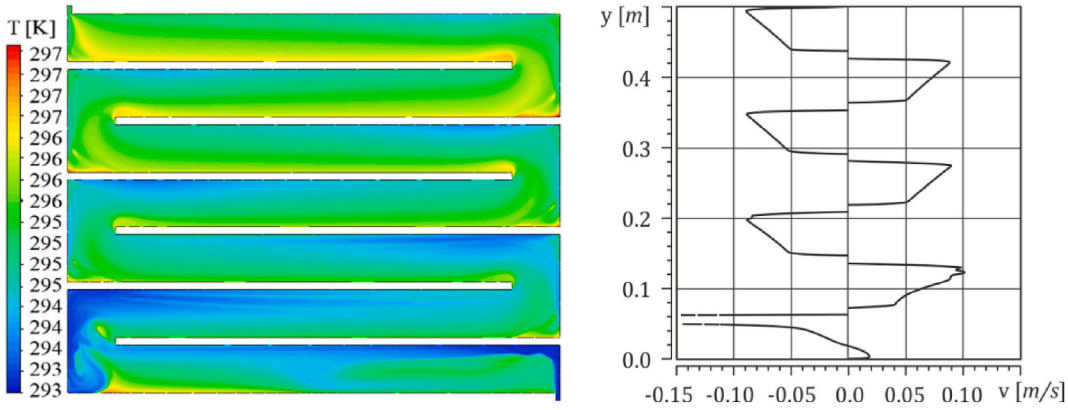

Fig. 5. *Temperature variation and velocity profile in the symmetry plane yoz for* DASCs with 6 ribs, $\dot{V}_3$

safety, charge and discharge valves (*V*), air separator, four temperature sensors (*T*) and an electronic control unit of fluid flow, which also allows remotely operation of the solar station. Data collected may be graphically displayed on computer using specific software. In order to have same temperature on inlet (T_{in}) for solar collectors, both of them are connected to a common indirect heater tank (*HT*) having a volume of 100 L of water and two integrated coiled tube heat exchangers, whose outlets are connected to inlets of the solar stations through two collecting tanks that operate under atmospheric pressure.

The control systems (Ekontrol) of the solar stations were employed to monitor the operating parameters for each solar collector during measurements: temperatures, flow rate and power consumed by the solar pump. A water flow sensor FS300A with a precision of 3 % was employed to control the flow rate. The temperature sensors (NTC10K-type, accuracy: ±0.7 °C) were installed as follows: two temperature sensors at inlet and outlet of solar collector, one temperature sensor on top surface of the collector and one sensor temperature inside the water heater. The solar station calibrates automatically the temperature sensors at the beginning of each measurement. In addition, solar irradiance, temperature and wind speed were monitored using a solar irradiance meter FLK-IRR1-SOL

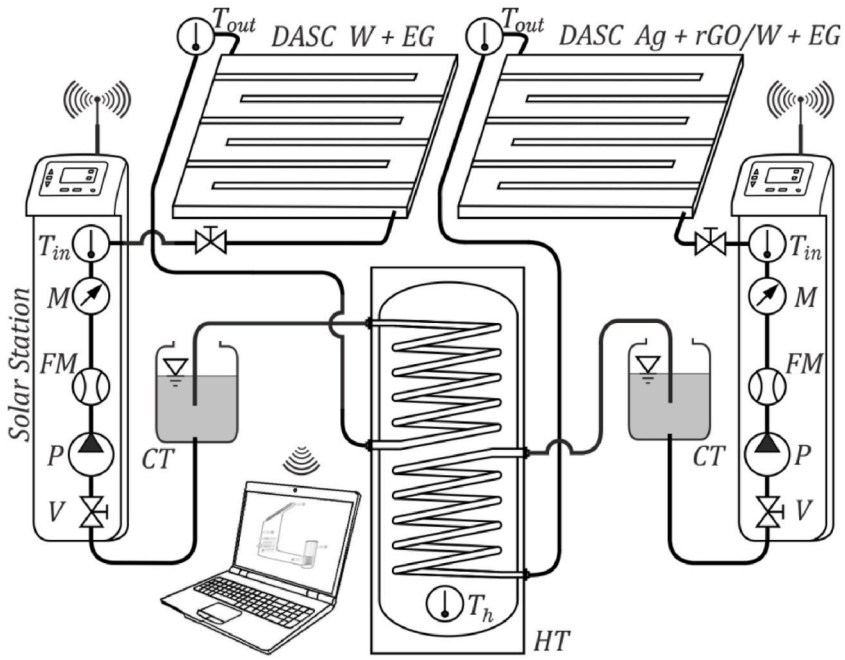

Fig. 6. Experimental layout for DASCs testing, M (manometer), FM (flow meter), P (pump), V (valve), HT (heater tank), CT (collecting tank).

having the precision of 5 %, respectively an anemometer KIMO AMI 300 with the precision of 2 %. Thus, the DASCs were tested in outdoor conditions of Brasov city, Romania, what is located in the center of the country, nearest to the 45th parallel north, at an average altitude of 625 m.

In the current study, the reliability of the two DASCs during long-time period has been analyzed for summer conditions. The study provides realistic data about the DASCs performance in a typical day of August 2023, between 11:00 a.m. and 4:00 p.m. local time. Weather values, temperature, wind speed, relative humidity in Brasov during this period are depicted in Fig. 7, according to recordings provided by Meteoblue, a weather forecast and data across the world.

Solar irradiance, ambient temperature and wind speed were recorded at 10 min interval, while temperatures values were monitored by Ekontrol systems. Experiments were conducted for an inlet temperature of 30 $^{\circ}C$, sated up according to the ambient temperature, and three flow rates of 0.5, 0.8 and 1 l/min.

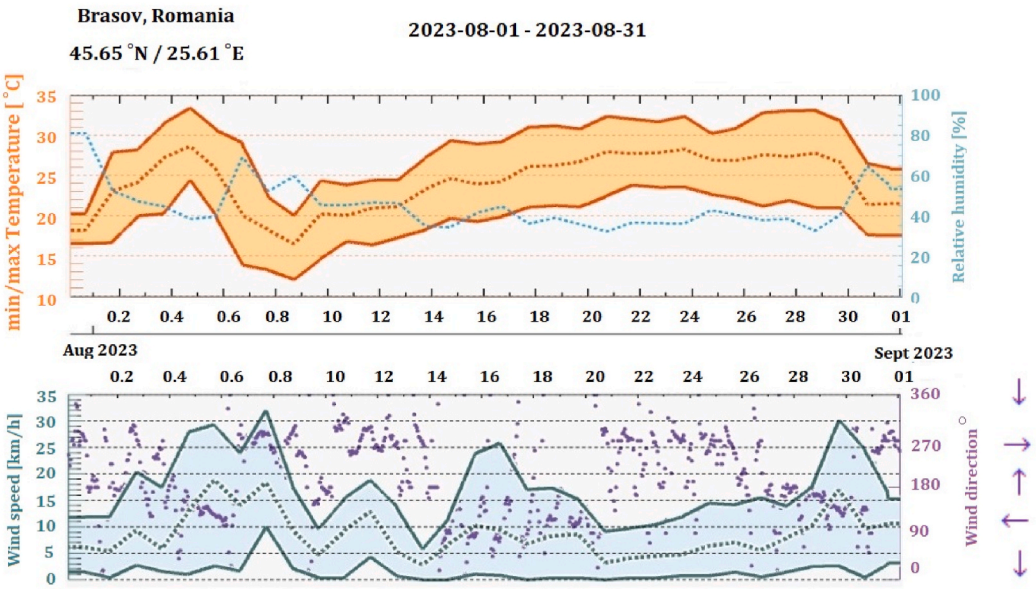

Fig. 7. The weather values in Brasov, August 2023.

Uncertainty of the efficiency of DASCs during experiments was computed by the root sum square method according to ISO/IEC GUIDE 98–3:2008(E), taking into account the precision of flow rate, temperature difference between inlet and outlet and solar irradiance

$$U_\eta = \sqrt{\sum U_i^2} = \sqrt{\left(\frac{\Delta \dot{V}}{\dot{V}}\right)^2 + \left(\frac{\Delta(T_{out} - T_{in})}{T_{out} - T_{in}}\right)^2 + \left(\frac{\Delta G_t}{G_t}\right)^2} \quad (7)$$

For all experiments, the average uncertainty calculated for the collectors' efficiency is 2.8 % with a maxim value of 4.0 %.

3.2. The working fluid

In the first stage, in order to have a reference, and also to validate the CFD study, one DASC filled with pure water was tested. Later, the performances of two DASCs were investigated simultaneously, one of them filled with a typical working fluid, respectively water-ethylene glycol solution (1:1), and the second one using the same base fluid with Ag NPs + rGO (1:1) hybrid nanofluid for a concentration of 0.1 wt%. The Ag NPs + rGO hybrid nanofluid was synthesized, characterized, and prepared following the detailed procedure by Huminic et al. [32,33]. Additionally, the stability studies of the hybrid nanofluid, including Zeta Potential, average hydrodynamic diameters (DLS), and pH-value were extensively presented in Huminic et al. [33].

In summary, as referenced in Refs. [32,33], the improved Hummer's graphite oxidation method was employed for the synthesis of graphene oxide, as the precursor for reduced graphene oxide. To prepare the aqueous silver ion solution, an amount of 0.1969 g AgNO3 was added to a mixture of 0.1 g of low-viscosity sodium carboxymethyl cellulose (CMCNa) and 50 g of distilled water. Then, the silver ion solution was mixed with the GO dispersion and with 0.4 g of aqueous solution of the reducing agent (NaBH4) using a mixing system. Stability studies led to the following results: average hydrodynamic diameter: 1497.2 nm, mean Zeta Potential: 11 mV, polydispersity index: 0.42 and pH: 8.42.

4. Results and discussion

Investigation of the two DASCs prototypes using water + ethylene glycol solution and 0.1 wt% Ag NPs + rGO hybrid nanofluid were conducted simultaneously for three values of flow rates within the range considered for CFD simulations, $\dot{V} = 0.5$, 0.8 and 1.0 l/min, according to standard EN-12975-2, what demandes a minimum time interval of 5 h for experiments and irradiance larger than 700 W/m^2, as emphasized in Table 1.

The measurements were carried out from 11:00 a.m. to 4:0 p.m. local time, taking into account that solar irradiance decreases after 4 p.m. as show in Fig. 11a in the case of DASC with water as working fluid.

4.1. DASCs efficiency

Figs. 8–10 depict the results of solar irradiance, ambient temperature, air speed, outlet temperature of the DASCs, water heater temperature and instantaneous efficiency for a typical day for considered flow rates. The inlet temperature for the DASCs collectors was set at 30 °C, considering the ambient temperature varied between 25 and 38 °C during the day. The solar irradiance was monitored on each collector. According to EN-12975-2, the instantaneous efficiency was computed with Eq. (3) for values of solar irradiance exceeding 700 W/m^2.

Fig. 8 (a, b, c) illustrates the effects of solar irradiance and the ambient temperature on the DASCs performance in the case of flow rate $\dot{V}_1 = 0.5\ l/min$. The ambient temperature varied within the interval [25, 35.1] $^\circ C$, and the air speed in the range [0, 2.5] m/s. The solar irradiance was from 450 W/m^2 at 11:00 a.m. to 1012 W/m^2 at 3:20 p.m. with two negative peaks at 2:30 p.m. (238 W/m^2 and 243 W/m^2) and 3:50 p.m. (235 W/m^2), due to some short periods of cloudy sky. As shown, the outlet temperature increases with both increasing solar irradiance and ambient temperature. For lower values of solar irradiance, the outlet temperatures increase nearly linearly. At higher solar irradiance values, the outlet temperature of the Ag NPs + rGO nanofluid shows more sensitivity to changes in solar irradiance compared to W + EG solution, with more pronounced fluctuations over time. During the test period, the water heater temperature increased by 8 $^\circ C$ from 30.5 $^\circ C$ to 38.5 $^\circ C$. Fig. 8c shows the variation of instantaneous efficiency for both DASCs during the measurements. As depicted, the efficiency significantly increases with the addition of small quantities of Ag NPs + rGO (0.1 wt%) to the base fluid. The average efficiency for DASC using W + EG solution was 19.87 %, and 31.5 % for those using Ag NPs + rGO nanofluid, emphasising an efficiency improvement of approximately 59 % with the nanofluid over the W + EG solution.

The solar irradiance, ambient temperature, air speed, outlet temperature of the DASCs, water heater temperature and the instantaneous efficiency for the second flow rate $\dot{V}_2 = 0.8\ l/min$ are depicted in Fig. 9 (a, b, c). The ambient temperature varied

Table 1
Test conditions for DASCs efficiency.

	EN-12975-2	*Test conditions*
Duration of exposure	>5 h	5 h
Global irradiance	>700 W/m^2	>700 W/m^2
Collector tilt angle	40° … 50°	45°

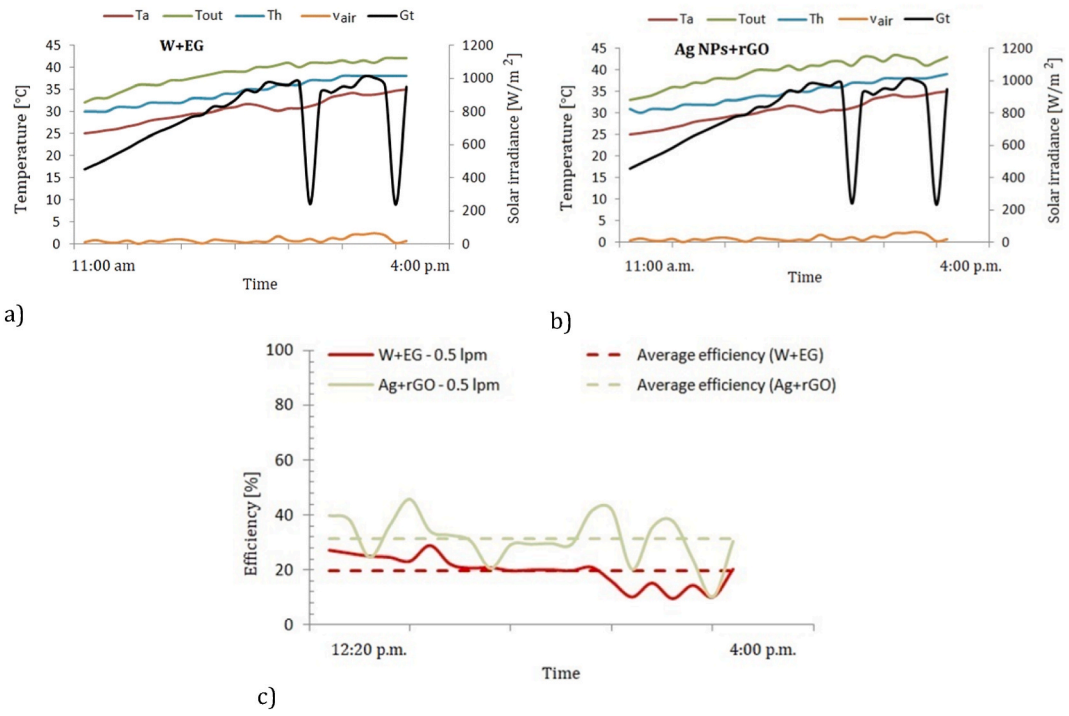

Fig. 8. *Parameters and efficiency of DASCs for* $\dot{V}_1 = 0.5\, l/min$

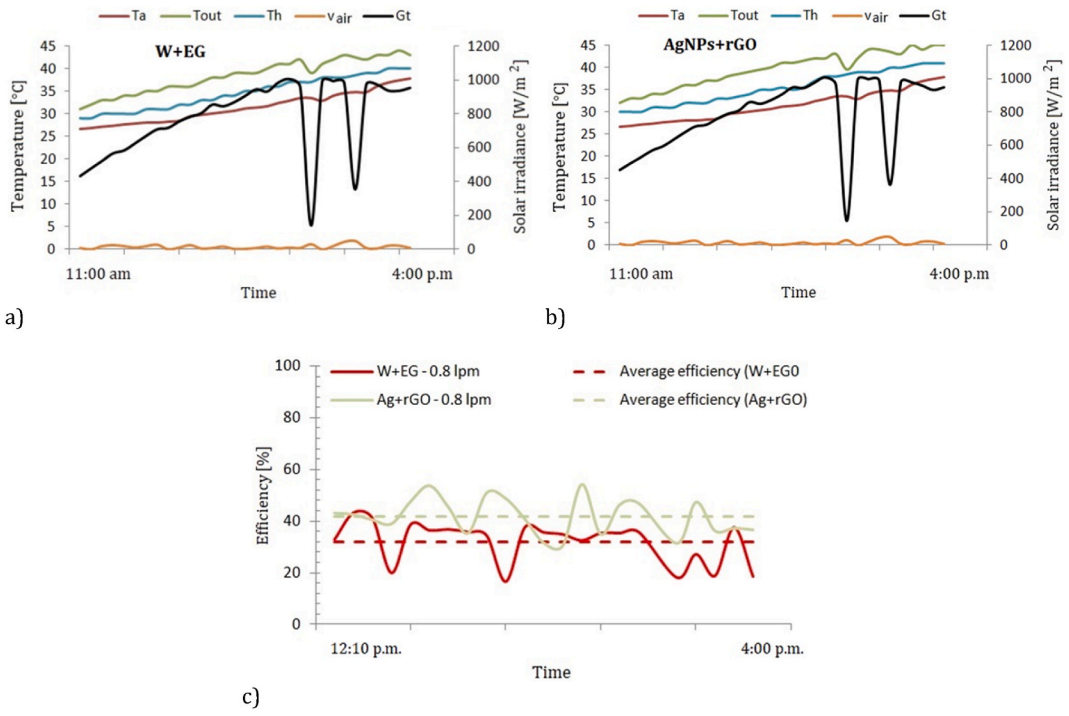

Fig. 9. *Parameters and efficiency of DASCs for* $\dot{V}_2 = 0.8\, l/min$

between 26.7 and 37.8 $^{\circ}C$ and the air speed values in the range 0 m/s to 1.8 m/s. The solar irradiance increased from 433 W/m^2 at 11:00 a.m. to 1005 W/m^2 at 2:10 p.m. with two negative peaks occurring at 2:30 p.m. (142 W/m^2 and 143 W/m^2) and 3:10 p.m. (355 W/m^2 and 360 W/m^2. As solar irradiance and ambient temperature rise, the outlet temperature of the DASCs also increases, as

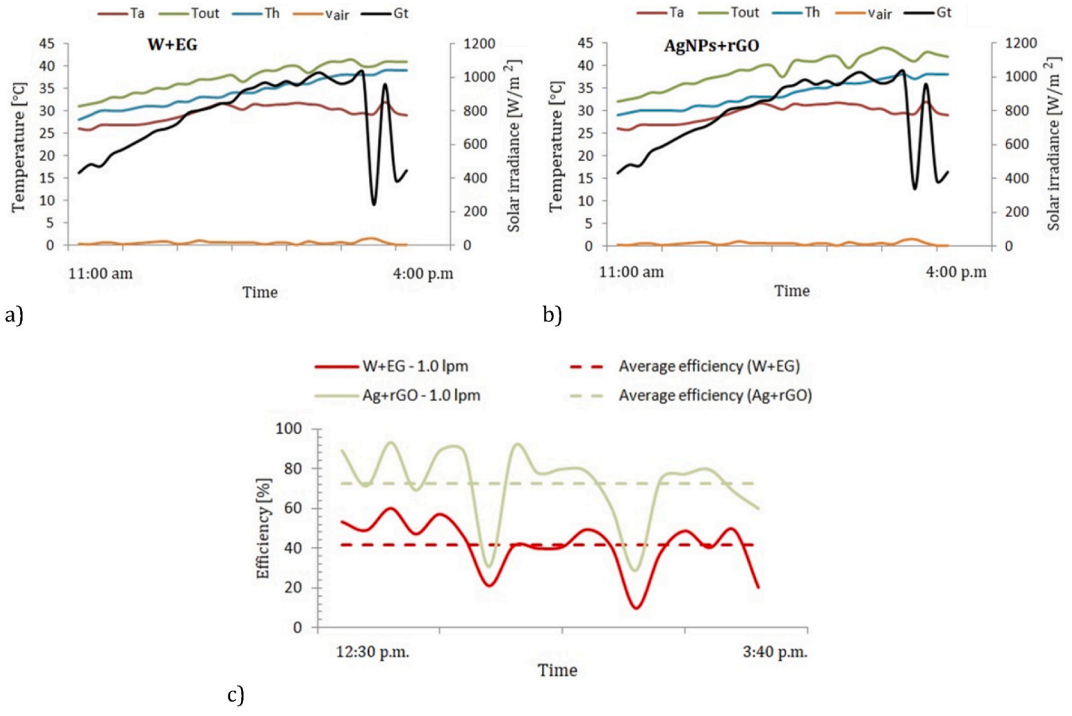

Fig. 10. *Parameters and efficiency of DASCs for* $\dot{V}_3 = 1.0\, l/min$

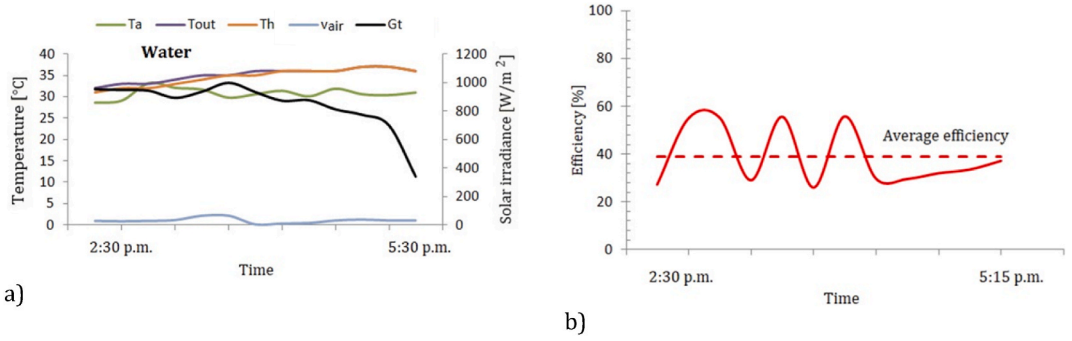

Fig. 11. *Measured parameters and efficiency of DASCs using water for* $\dot{V} = 1.1\, l/min$

illustrated in Fig. 9(a and b). An increase in ambient temperature leads to an average increase in the outlet temperature by about 1.5 °C compared to the measurements conducted at a flow rate of 0.5 l/min. At the same time, it can be seen that decrease in the solar irradiance over short periods of time, approximately 10 min, also influences the outlet temperature of the working fluid. By increasing flow rate from 0.5 l/min to 0.8 l/min, the water heater temperature increased by 11 °*C*, from 29.5 °*C* to 40.5 °*C*. The instantaneous efficiency of the DASCs during experiments for a solar irradiance higher than 700 W/m^2 is illustrated in Fig. 9c. It can be seen that the average efficiency increases with the flow rate. The average efficiency values for DASCs using W + EG solution and Ag NPs + rGO nanofluid were 31.86 % and 41.86 % respectively, resulting in a efficiency improvement of about 31.4 % by using Ag NPs + rGO nanofluid. It has also been observed that an increase in flow rate enhances the average efficiency, although the rate of improvement diminishes as the flow rate continues to increase.

Fig. 10 (a, b, c) depicts measurements results for the third flow rate, $\dot{V}_3 = 1.0\, l/min$. The ambient temperature increases from 26.7 °*C* to 31.8 °*C* and the air speed was within the range [0, 1.1] m/s. The solar irradiance varied from 430 W/m^2 at 11:00 a.m. to 1030 W/m^2 at 3:20 p.m., with three negative peaks at 3:30 p.m. (240 W/m^2 and 340 W/m^2), 3:50 p.m. (390 W/m^2) and 4:00 p.m. (444 W/m^2 and 430 W/m^2). Similar behaviour in terms of temperatures and solar irradiance may be seen also for these measurements, as shown in Fig. 10(a and b). The outlet temperature of DASCs is influenced by the ambient temperature and solar irradiance during experiments. By increasing the flow rate, the water heater temperature increased by 10 °*C* from 28.5 °*C* to 38.5 °*C*, under the conditions in which the average ambient temperature was lower with 5 °*C* than in previous days. Under these testing conditions, the average efficiency values

for DASCs employing W + EG solution and Ag NPs + rGO nanofluid were 41.73 % and 72.65 % respectively, indicating an enhancement in DASC efficiency of approximately 74.09 % by using Ag NPs + rGO nanofluid, as shown in Fig. 10c. The average efficiency of the DASC using nanofluid follows a similar trend to that of the base fluid, W + EG solution. The minimum efficiency values occur at a flow rate of 0.5 l/min, while the maximum values are observed at 1.0 l/min.

As mentioned previously, an initial test was also performed for a DASC using water as the working fluid, in similar conditions as in numerical computations for a flow rate of 1.1 l/min, during a time interval from 2:30 p.m. to 5:30 p.m., in order to validate the CFD simulations, and also to have a reference for current investigations. Fig. 11a depicts the measured parameters during this experiment. As shown, the ambient temperature varied between 28.6 $°C$ and 33.2 $°C$, while the air speed values are within the range [0.1, 2.1] m/s. During this test, the water heater temperature increased by 5 $°C$ from 31 $°C$ to 36 $°C$. The instantaneous efficiency variation of the DASC is illustrated in Fig. 11b, with an average efficiency value of 38.87 %.

The average efficiency values as function of flow rate for all tested working fluids is shown in Fig. 12. As seen, the efficiency of the DASC using water is about 7 % lower than that of the DASC collector using W + EG solution at a flow rate of 1.0 l/min. Furthermore, it has been noted that Ag NPs + rGO nanofluid possesses a strong absorption capacity for solar energy, which substantially improves the efficiency of DASCs across all examined flow rates.

An increase in flow rate intensifies the heat transfer between the working fluid and DASCs walls. In the DASC using Ag + rGO nanofluid, a part of the absorbed heat by the DASC surface is transferred to the nanofluid and a smaller amount of heat is reflected to the environment. By increasing flow rate and the intensification of heat transfer, the nanofluid absorbs more heat, leading to improving of efficiency. As a result of the measurements carried out, it can be stated that the DASC efficiency depends on the way it is design, its configuration, the materials used in its manufacture and the used working fluid.

4.2. Instantaneous and accumulative energies

The instantaneous energy delivered to the system by both the DASCs using W + EG solution and Ag NPs + rGO nanofluid for all studied flow rates is shown in Fig. 13 (a, b, c). The results reveal a marked enhancement in performance of the DASC prototype employing Ag NPs + rGO nanofluid over the one with W + EG solution. For all three flow rates, the maximum useful energies are 241.71 W/m2, 349.11 W/m2 and 484.98 W/m2 for DASC in the case of W + EG base solution, while for DASC using Ag NPs + rGO nanofluid, the maximum useful energies are 383.91 W/m2, 519 W/m2 and 862.84 W/m2, showing thus a maximum improvement of 43.8 %.

Fig. 14 (a, b, c) depict accumulative energy delivered to the system by DASCs using both W + EG solution and Ag NPs + rGO nanofluid during experiments for flow rates. These results unveil that in the same time interval, the DASC using Ag NPs + rGO nanofluid achieved a maximum accumulative energy delivered of 1.44 kWh/m^2, 1.84 kWh/m^2 and 3.07 kWh/m^2 for flownrates of 0.5 l/min, 0.8 l/min and 1.0 l/min respectively. For the same flow rates, the DASC with W + EG solution reached the following maximum values of accumulative energy: 0.97 kWh/m2, 1.4 kWh/m2, and 1.55 kWh/m2. Thus, the accumulative energy delivered by the DASC prototype using Ag NPs + rGO nanofluid is twice than provided by the DASC using W + EG solution at a flow rate of 1.0 l/min, demonstrating the superior efficiency of this nanofluid in DASC applications and its applicability in solar collectors.

4.3. Heat losses

In the design process of solar collectors, it is crucial to consider the reduction of heat losses. These losses can occur through convection, as wind passes over the collector's upper surface, through radiation, and also through conduction from the collector's back and sides. Fig. 15 (a, b, c) shows the heat losses computed as $Q_{loss} = \mathrm{A}\ G_t - \dot{Q}_u$ for different flow rates during experiments. Analyzing these results, it can be seen that the heat losses through the collector are directly influenced by the solar irradiance and the ambient temperature. Thus, at the beginning of the measurements when both solar irradiance and ambient temperature are lower, heat losses diminish, and the absorptivity of the DASCs enhances. Conversely, as solar irradiance and ambient temperature rise, radiation heat losses intensify. These findings also demonstrate that DASCs using Ag NPs + rGO outperform those using W + EG solution. Additionally, it has been noticed that an increase in flow rate leads to reduced heat losses (Fig. 16), and consequently, to enhanced performance of DASCs. Hence, the DASCs solar collectors can constitute a novel technology for converting solar energy into thermal

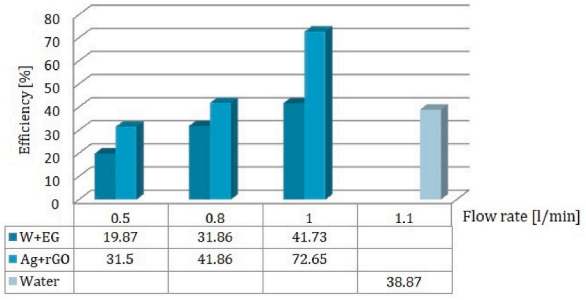

Fig. 12. Average efficiency of DASCs using water, W + EG solution and AgNPs + rGO nanofluid.

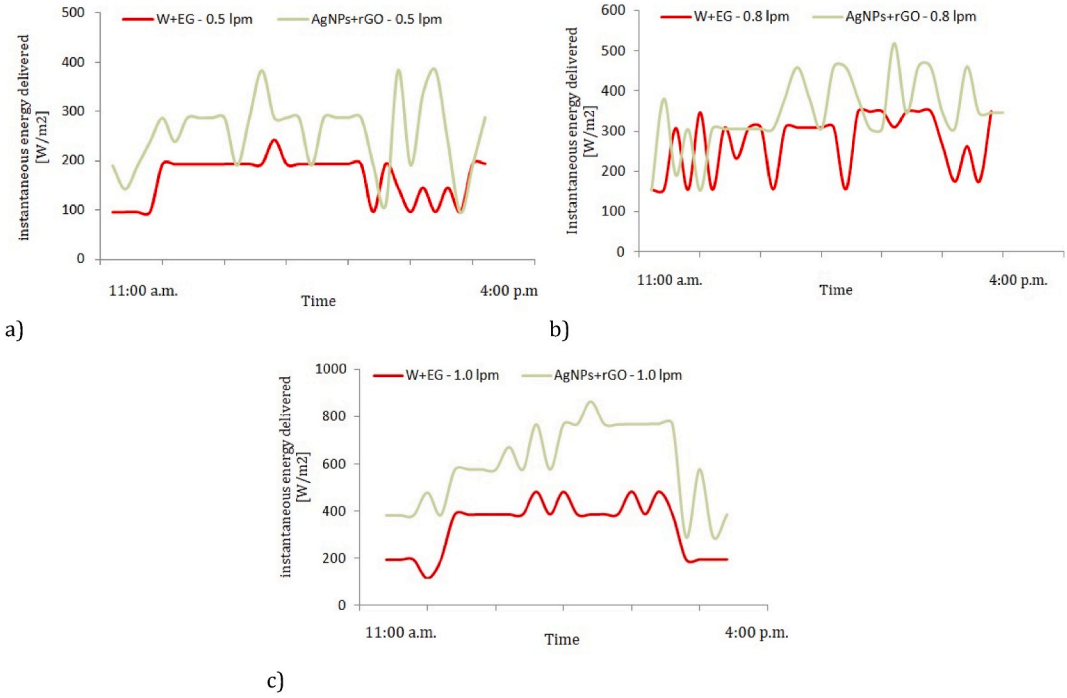

Fig. 13. The instantaneous energy delivered during experiments.

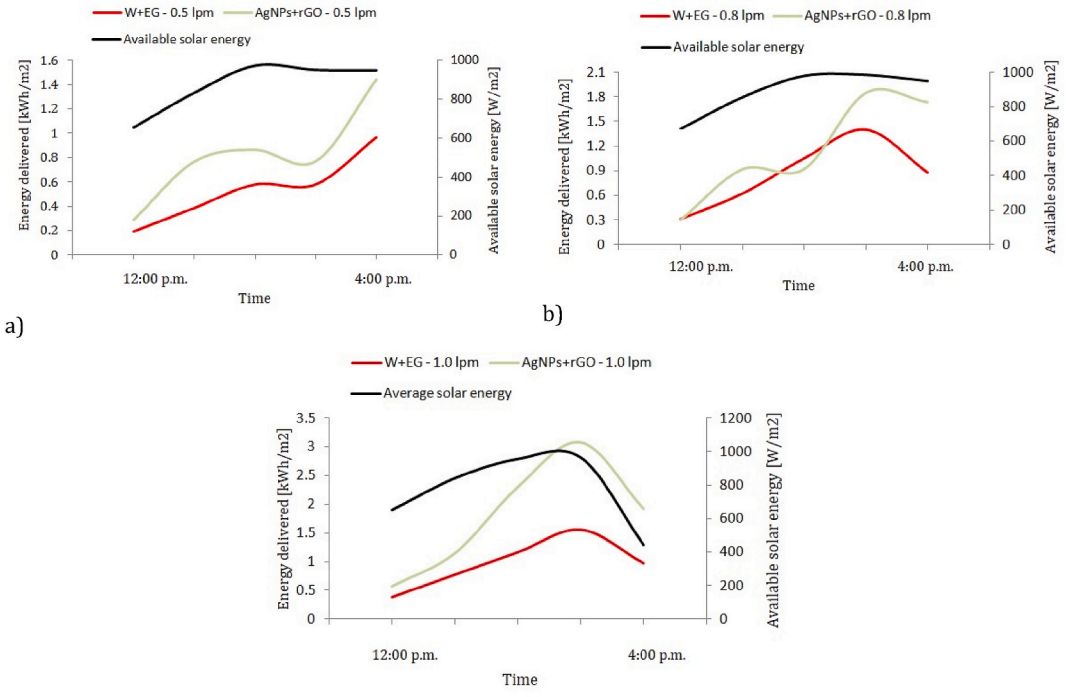

Fig. 14. Accumulative energy delivered during measurements.

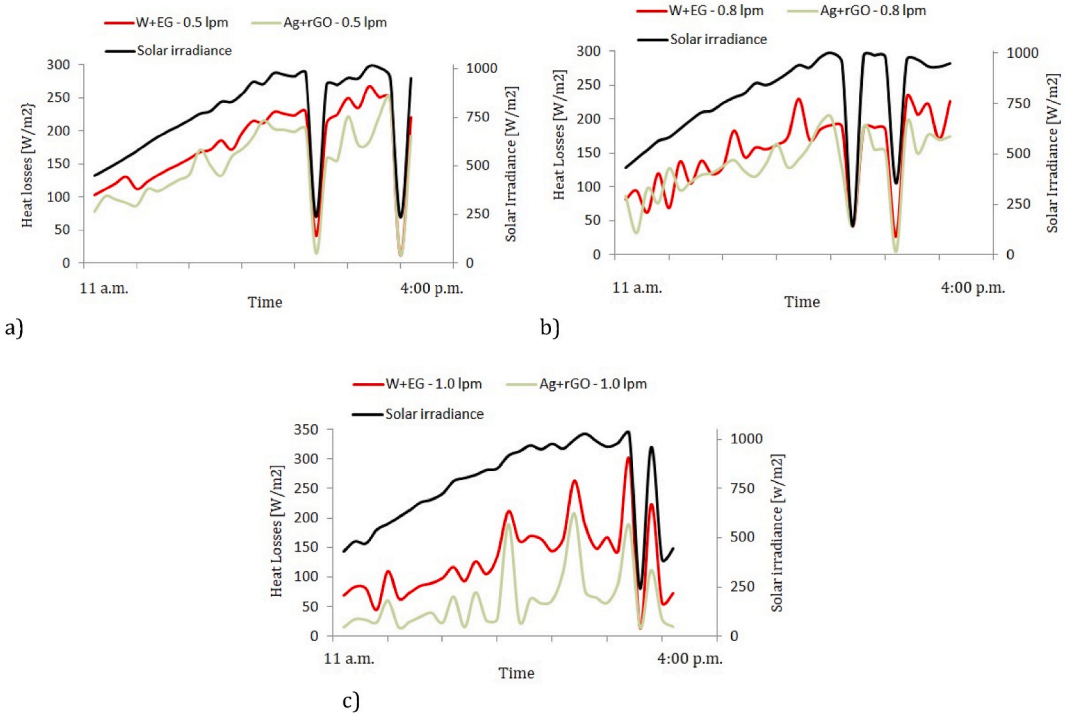

Fig. 15. Heat losses for considered flow rates.

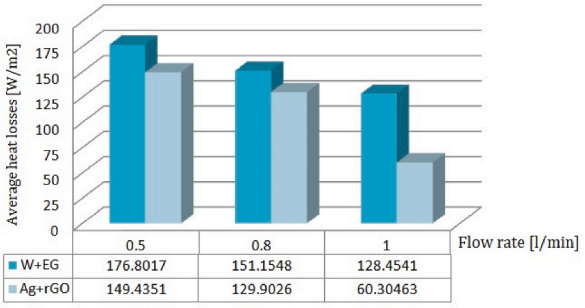

Fig. 16. Average heat losses for considered flow rates.

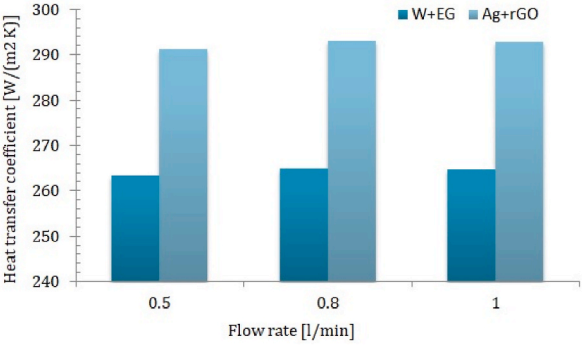

Fig. 17. The convective heat transfer coefficients inside of collector as a function of flow rate.

energy.

4.4. Heat transfer coefficients

The Nusselt number inside the DASC as given by Ref. [34] is:

$$Nu = \frac{(h_{c,i})D_h}{k} = 7.54 + \frac{0.03\left(\frac{D_h}{L}\right)Re\,Pr}{1 + 0.06\left[\left(\frac{D_h}{L}\right)Re\,Pr\right]^{2/3}} \tag{8}$$

where the hydraulic diameter is twice the thickness of the collector.

Fig. 17 illustrates the convective heat transfer coefficient for both W + EG solution and Ag NPs + rGO hybrid nanofluid, for studied flow rates. As depicted, the heat transfer coefficients for the hybrid nanofluid are significantly larger than those for W + EG solution, with an enhancement nearly 10.6 % (10.61 %, 10.68 %, and 10.59 % respectively).

The heat transfer coefficient from top glazing to the surrounding was estimated by using Eq. (9) and the results were illustrated in Fig. 18.

$$h = h_c + h_r = (2.8 + 3\,\mathrm{v}) + \sigma\,\varepsilon_g\left(T_g^2 + T_a^2\right)\left(T_g + T_a\right) \tag{9}$$

Since the DASCs were tested simultaneously, the convection heat transfer coefficients for both W + EG solution and the Ag NPs + rGO hybrid nanofluid are identical, given the wind speed values are the same. Consequently, it can be seen that the DASC with Ag NPs + rGO suspension absorbs more solar energy than that with W + EG solution, due to the greater influence of the radiation heat transfer coefficient over the convection heat transfer coefficient.

Based on experimental data collected, a new correlation for the average Nusselt number is proposed

$$Nu = 7.225 \cdot Re^{0.017} \cdot Pr^{0.085} \cdot \left(\frac{D_h}{L}\right)^{0.045} \cdot (\sin\theta)^{0.25}, \tag{10}$$

for the following conditions: $0.5\,l/min < \dot{V} < 1.0\,l/min$, $0.015 < D_h/L < 0.046$, $\sin\theta = 40^\circ$ şi 45°. The deviations between the experimental data and those calculated using Eq. (10) are within the range $-7.15\,\%\ldots+6.28\,\%$.

4.5. Comparison of current results to experimental data carried out at full-scale DASCs

The DASC prototype developed in this study, optimized through CFD simulations and experimentally validated under real outdoor conditions, offers several key advantages. By incorporating ribbed flow channels and a novel Ag NPs–rGO/water-ethylene glycol hybrid nanofluid, the system achieved a maximum efficiency of 72.65 % at a flow rate of 1.0 l/min (equivalent to 0.01763 kg/s). This performance is competitive with that reported in earlier studies: Karami et al. [35] and Delfani et al. [17] observed efficiencies ranging from 64.7 % to 89.3 % for CuO- and MWCNT-based DASCs at mass flow rates between 0.015 and 0.025 kg/s. Similarly, Karami et al. [24] examined hybrid Fe_3O_4/SiO_2 nanofluids, reporting efficiency values between 58 % and 92 % for flow rates from 0.0075 to 0.0225 kg/s. It is important to note that these studies were conducted in Iran, a region with significantly more favorable solar irradiance compared to Romania, where the present study was carried out. Despite the less favorable climatic conditions, the proposed DASC still achieved high efficiency, underlining both the robustness of the design and the effectiveness of the selected hybrid nanofluid. This makes the current system particularly promising for solar thermal applications in moderate solar resource regions.

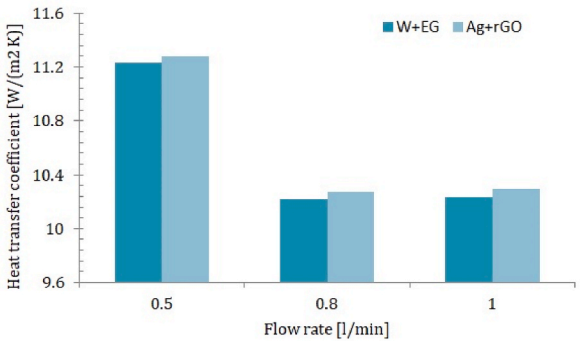

Fig. 18. The heat transfer coefficients from top glazing to the surrounding as function of flow rate.

5. Conclusions

In the current paper, new DASCs prototypes using water + ethylene mixture (W + EG (1:1)) and 0.1 wt% Ag NPs + rGO (1:1)/W + EG hybrid nanofluid were design, optimized and investigated numerically and experimentally. The experiments were conducted simultaneously for three flow rates of 0.5 l/min, 0.8 l/min, and 1.0 l/min in the time interval 11:00 a.m. to 4:0 p.m. (local time) according to the Standard EN-12975-2. Based on experimental analysis, the following conclusions may be outlined:

- The DASCs efficiency exhibits an increasing trend with increasing flow rate. For DASC prototype using W + EG solution, the maximum average efficiency was 41.73 % at a flow rate of 1.0 l/min. At the same flow rate, the maximum average efficiency of DASC prototype using Ag NPs + rGO nanofluid was 72.65 %. The maximum efficiency enhancement was 74.09 % compared to the base fluid;
- The efficiency values of the two DASCs prototypes were higher than the efficiency of DASC using water at 1.1 l/min;
- During testing period, the water temperature in the heater (100 L) increased by a maximum 11 °C, reaching 40.5 °C;
- The maximum improvement in instantaneous energy delivered was 43.8 % for DASC using AgNPs + rGO nanofluid at 1.0 l/min compared to the base fluid;
- The maximum improvement in accumulative energy delivered was 98.06 % for DASC using AgNPs + rGO nanofluid at 1.0 l/min compared to the base fluid;
- With increasing flow rate the heat losses were reduced. The heat losses of DASC using AgNPs + rGO nanofluid were lower than those of DASC using W + EG solution.
- The use of AgNPs + rGO nanofluid improves the convective heat transfer coefficient by about 11.0 %.

These new DASCs prototypes solar collectors constitute a new technology for the conversion of solar energy into thermal energy with improved performance. Future research will focus on optimizing this new type of collector and testing several types of hybrid nanofluids.

CRediT authorship contribution statement

Angel Huminic: Writing – review & editing, Writing – original draft, Validation, Supervision, Methodology, Investigation, Formal analysis, Data curation, Conceptualization. **Gabriela Huminic:** Writing – review & editing, Writing – original draft, Validation, Supervision, Resources, Project administration, Methodology, Investigation, Funding acquisition, Formal analysis, Data curation, Conceptualization.

Declaration of competing interest

The authors declare that they have no known competing financial interests or personal relationships that could have appeared to influence the work reported in this paper.

Acknowledgments

This work was supported by grants from the Romanian Ministry of Education and Research, CNCS-UEFISCDI, projects number PN-III-P4-ID-PCE-2020-0353.

Data availability

Data will be made available on request.

References

[1] A. Huminic, G. Huminic, C. Fleacă, F. Dumitrache, I. Morjan, Thermo-physical properties of water based lanthanum oxide nanofluid. An experimental study, J. Mol. Liq. 287 (2019) 11013.
[2] G. Huminic, A. Huminic, F. Dumitrache, C. Fleaca, I. Morjan, Experimental Study of thermo-physical properties of nanofluids based on γ-Fe_2O_3 nanoparticles for heat transfer applications, Heat Transf. Eng. 38 (2017) 1496–1505.
[3] A. Vărdaru, G. Huminic, A. Huminic, C. Fleacă, F. Dumitrache, I. Morjan, Synthesis, characterization and thermal conductivity of water based graphene oxide–silicon hybrid nanofluids: an experimental approach, Alex. Eng. J. 61 (2022) 12111–12122.
[4] A. Mashhadian, M.M. Heyhat, O. Mahian, Improving environmental performance of a direct absorption parabolic trough collector by using hybrid nanofluids, Energy Convers. Manag. 244 (2021) 114450.
[5] Z. Li, An Kan, K. Wang, Y. He, N. Zheng, W. Yu, Optical properties and photothermal conversion performances of graphene based nanofluids, Appl. Therm. Eng. 203 (2022) 117948.
[6] T.P. Otanicar, P.E. Phelan, R.S. Prasher, G. Rosengarten, R.A. Taylor, Nanofluid-based direct absorption solar collector, J. Renew. Sustain. Energy 2 (2010) 033102.
[7] T. Otanicar, R.A. Taylor, P.E. Phelan, R. Prasher, Impact of size and scattering mode on the optimal solar absorbing nanofluid, in: ASME 2009 3rd International Conference on Energy Sustainability, vol. 1, ASMEDC, San Francisco, California, USA, 2009, pp. 791–796.
[8] R.A. Taylor, P.E. Phelan, T.P. Otanicar, C.A. Walker, M. Nguyen, S. Trimble, R. Prasher, Applicability of nanofluids in high flux solar collectors, J. Renew. Sustain. Energy 3 (2011) 023104.
[9] S.M. Ladjevardi, A. Asnagh, P.S. Izadkhast, A.H. Kashani, Applicability of graphite nanofluids in direct solar energy absorption, Sol. Energy 94 (2013) 327–334.

[10] Z. Luo, C. Wang, W. Wei, G. Xiao, M. Ni, Performance improvement of a nanofluid solar collector based on direct absorption collection (DAC) concepts, Int. J. Heat Mass Tran. 75 (2014) 262–271.
[11] T.B. Gorji, A.A. Ranjbar, Geometry optimization of a nanofluid-based direct absorption solar collector using response surface methodology, Sol. Energy 122 (2015) 314–325.
[12] T.B. Gorji, A.A. Ranjbar, A numerical and experimental investigation on the performance of a low-flux direct absorption solar collector (DASC) using graphite, magnetite and silver nanofluids, Sol. Energy 135 (2016) 493–505.
[13] T.B. Gorji, A.A. Ranjbar, Thermal and exergy optimization of a nanofluid-based direct absorption solar collector, Renew. Energy 106 (2017) 274–287.
[14] J. Liu, Z. Ye, L. Zhang, X. Fang, Z. Zhang, A combined numerical and experimental study on graphene/ionic liquid nanofluid based direct absorption solar collector, Sol. Energy Mater. Sol. Cells 136 (2015) 177–186.
[15] M. Vakili, S.M. Hosseinalipour, S. Delfani, S. Khosrojerdi, M. Karami, Experimental investigation of graphene nanoplatelets nanofluid-based volumetric solar collector for domestic hot water systems, Sol. Energy 131 (2016) 119–130.
[16] B. Filho, E. Pedone, Experimental investigation of a silver nanoparticle-based direct absorption solar thermal system, Energy Convers. Manag. 84 (2014) 261–267.
[17] S. Delfani, M. Karami, M.A. Akhavan- Behabadi, Performance characteristics of a residential-type direct absorption solar collector using MWCNT nanofluid, Renew. Energy 87 (2016) 754–764.
[18] M. Karami, M. Bozorgi, S. Delfani, M.A. Akhavan-Behabadi, Empirical correlations for heat transfer in a silver nanofluid-based direct absorption solar collector, Sustain. Energy Technol. Assessments 28 (2018) 14–21.
[19] P.G. Struchalin, V.S. Yunin, K.V. Kutsenko, O.V. Nikolaev, A.A. Vologzhannikova, M.P. Shevelyova, O.S. Gorbacheva, B.V. Balakin, Performance of a tubular direct absorption solar collector with a carbon-based nanofluid, Int. J. Heat Mass Tran. 179 (2021) 121717.
[20] S. Kumar, V. Sharma, M.R. Samantaray, N. Chander, Experimental investigation of a direct absorption solar collector using ultra stable gold plasmonic nanofluid under real outdoor conditions, Renew. Energy 162 (2020) 1958–1969.
[21] Sujit Kumar Verma, Arun Kumar Tiwari, Sandeep Tiwari, Durg Singh Chauhan, Performance analysis of hybrid nanofluids in flat plate solar collector as an advanced working fluid, Sol. Energy 167 (2018) 231–241.
[22] A.M. Ajeena, I. Farkas, P. Víg, Performance enhancement of flat plate solar collector using ZrO2-SiC/DW hybrid nanofluid: a comprehensive experimental study, Energy Convers. Manag. X 20 (2023) 100458.
[23] Z.A. Alrowaili, M. Ezzeldien, N.M. Shaaalan, E. Hussein, M.A. Sharafeldin, Investigation of the effect of hybrid CuO-cu/Water nanofluid on the solar thermal energy storage system, J. Energy Storage 50 (2022) 104675.
[24] M. Karami, Experimental investigation of first and second laws in a direct absorption solar collector using hybrid Fe_3O_4/SiO_2 nanofluid, Journal of Thermal Analysis and Calorimetry 136 (2019) 661–671.
[25] A.A. Hachicha, Z. Said, Numerical modeling and multi-objective optimization of direct absorption solar collectors using Mono and hybrid nanofluids, J. Clean. Prod. 414 (2023) 137740.
[26] Z. Said, M. Ghodbane, L.S. Sundar, A.K. Tiwari, M. Sheikholeslami, B. Boumeddane, Heat transfer, entropy generation, economic and environmental analyses of linear fresnel reflector using novel rGO-Co_3O_4 hybrid nanofluids, Renew. Energy 165 (2021) 420e437.
[27] X. Li, G. Zeng, X. Lei, The stability, optical properties and solar-thermal conversion performance of SiC-MWCNTs hybrid nanofluids for the direct absorption solar collector (DASC) application, Sol. Energy Mater. Sol. Cell. 206 (2020) 110323.
[28] Y. Bao, A. Huang, X. Zheng, G. Qin, Enhanced photothermal conversion performance of MWCNT/siC hybrid aqueous nanofluids in direct absorption solar collectors, J. Mol. Liq. 387 (2023) 122577.
[29] S.K. Hazra, M. Michael, T.K. Nandi, Investigations on optical and photo-thermal conversion characteristics of BN-EG and BN/CB-EG hybrid nanofluids for applications in direct absorption solar collectors, Sol. Energy Mater. Sol. Cell. 230 (2021) 111245.
[30] X. Zuo, L. Song, W. Yang, Z. Zhang, X. Gao, J. Zhan, S. Wu, X. Wang, W. Zhu, H. Li, D. Zhang, H. Yin, Hua Yan, Y. An, Silicon dioxide coating nanocomposites and cellulose-modified stable nanofluid for direct absorption solar collection, Sol. Energy 262 (2023) 111797.
[31] V.K. Gupta, S. Kumar, R. Kukreja, N. Chander, Experimental thermal performance investigation of a direct absorption solar collector using hybrid nanofluid of gold nanoparticles with natural extract of Azadirachta indica leaves, Renew. Energy 202 (2023) 1021–1031.
[32] G. Huminic, A. Huminic, A. Vărdaru, F. Dumitrache, C. Fleacă, Experimental investigation on Ag NPs-rGO-water/ethylene-glycol hybrid nanofluids used in solar applications, Diam. Relat. Mater. 143 (2024) 110851.
[33] G. Huminic, A. Huminic, A. Vărdaru, C. Fleacă, F. Dumitrache, I. Morjan, Surface tension of Ag NPs-rGO based hybrid nanofluids, J. Mol. Liq. 390 (2023) 123002.
[34] Y.A. Cengel, Heat Transfer: a Practical Approach, second ed., Mc Graw-Hill, 2002.
[35] M. Karami, M.A. Akhavan-Bahabadi, S. Delfani, M. Raisee, Experimental investigation of CuO nanofluid-based direct absorption solar collector for residential applications, Renew. Sustain. Energy Rev. 52 (2015) 793–801.